

# Layered Uploading for Quantum Convolutional Neural Networks

Grégoire Barrué and Tony Quertier

## Abstract

Continuing our analysis of quantum machine learning applied to our use-case of malware detection, we investigate the potential of quantum convolutional neural networks. More precisely, we propose a new architecture where data is uploaded all along the quantum circuit. This allows us to use more features from the data, hence giving to the algorithm more information, without having to increase the number of qubits that we use for the quantum circuit. This approach is motivated by the fact that we do not always have great amounts of data, and that quantum computers are currently restricted in their number of logical qubits.

## Introduction

A lot of work has been done on parameterized quantum circuit in order to understand their capacities especially for quantum machine learning applications [5]. Expressiveness and generalization capabilities have been theoretically explored [1, 12, 26], enlightening some specific issues to the quantum setting. One of the most important issue seems to be the Barren Plateau phenomenon [10, 16], where gradients vanish exponentially fast with the increase of the number of qubits, causing the failure of the algorithm's learning. It turns out that the Lie algebra is an important tool to evaluate whether a quantum neural network is subject to Barren plateaus or not [24, 29], and some initialization strategies have been tested [8], as approaches to keep track of the data all along the circuits [19]. A particular alternative is also quantum convolutional neural networks (QCNNs) because it has been proved that under some hypothesis they do not exhibit Barren Plateaus [20]. They were first introduced in [6], and used for instance in [11] for classical data classification, or in [4] for multi-class classification. Their full understanding is still missing, but some works, as [28], start to deeply analyze these models, and we think that it could be a suitable solution for image classification, as is its classical equivalent.

This classification task is a big interest for us, as we want to use it for malware detection, which is a current area of research due to the ever-increasing number of attacks. In this context, researchers have turned to artificial intelligence to improve the detection of new malware [7, 23, 27], and some techniques have been developed to learn about features extracted from binary semantic and statistical

data [2], to use language processing elements [22] or even convolutional neural networks (CNNs) [14, 15].

In this article, we propose a new architecture for quantum convolutional networks, allowing to inject more features in the QCNN, and thus more information about the data, without increasing its size. We compare this architecture with a standard QCNN on two different datasets, first the well-known MNIST dataset and second a dataset composed of images corresponding to malware and benign PE files. Our motivation here is to prove that there are solutions to use more information in cases where great amounts of data are not available, or computations resources are limited. Thus we use relatively few data and models with little numbers of qubits.

This article is organized as follows. In Section 1 we detail the datasets that we use, especially the dataset containing malware files. We explain the preprocessing that we used, named Grayscale method, which allows to turn a PE file into an image, in order to perform image classification. Then Section 2 details the implementation of the standard quantum convolutional neural network that we use for our tests, and states the absence of Barren plateaus for this model. Finally Section 3 proposes our new architecture, layered uploading, and gathers the results of our experiments to highlight the efficiency of this method.

## 1 Preprocessings and datasets

Our principal interest is to study malware detection. In this aim we rely on two different datasets, Bodmas [30] and PEMachineLearning [13]. They all contain malicious and benign Portable Executable (PE) files, distribution and format are summarized in Table 1.

Table 1: Distribution and format of each dataset

| Dataset            | Malicious files | Benign files |
|--------------------|-----------------|--------------|
| Bodmas             | 57,293          | 77,142       |
| PEMachine Learning | 114,737         | 86,812       |

Bodmas [30] provided us a dataset composed of 134,435 binary files with pre-extracted features together with the 57,293 malicious files in raw PE format. These files have been collected during one year between August 2019 and September 2020 and labeled: authors indicate the category each file belongs to. The other dataset, PEMachineLearning is composed of 201,549 binary files including 114,737 malicious files. These files have been gathered from different sources such as VirusShare<sup>1</sup>, MalShare<sup>2</sup> and TheZoo<sup>3</sup>.

The preprocessing that we use in this work is based on the Grayscale method, which was initially submitted by Nataraj and al. [18] and converts a binary file

---

<sup>1</sup><https://virusshare.com/>

<sup>2</sup><https://malshare.com/>

<sup>3</sup><https://github.com/ytisf/theZoo>

into an image, as can be seen in Figure 1. To train our models, we choose to resize Grayscale images to  $64 \times 64$  pixels.

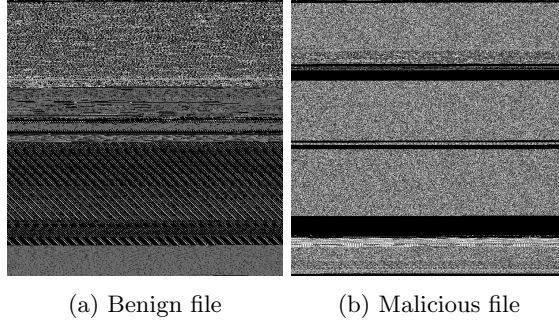


Figure 1: Example of PE files transformation into grayscale images

We also used the MNIST dataset in order to make sure that our algorithms works efficiently and that the method that we propose in this article is well illustrated. We also resize the images from the MNIST dataset to the  $64 \times 64$  size. From our dataset, we first extract only images labeled by '0' or '1', in order to compute a bipartite classification model. Then we also test our algorithm for images labeled by '0' and '8' which are more similar numbers, to challenge the efficiency of our model.

## 2 Descripton of the QCNN

A QCNN is an algorithm composed of an encoding layer, several convolutional and pooling layers, and finally a measurement operator, called observable. Figure 2 presents an example of such an algorithm with three layers, where  $U_\phi$  corresponds to the encoding layers,  $C_i$  correspond to the gates composing one convolutional layer and  $P_i$  correspond to the gates composing one pooling layer,  $i = 1, 2, 3$ . In our case the observable is the Z-measurement.

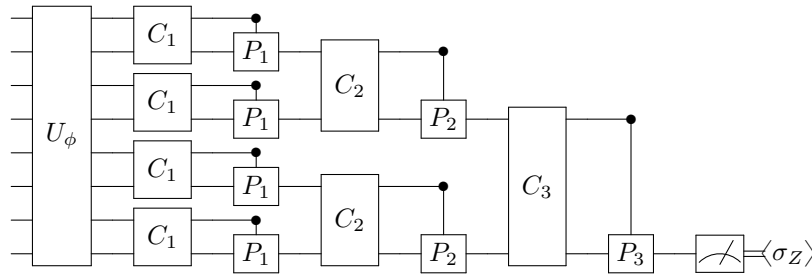


Figure 2: Standard architecture of a quantum convolutional neural network, where convolutional and pooling layers alternate up to the measurement by an observable.

Then, one can choose between several architectures for the convolutional layers, as for the pooling layers and the encoding map.

### Encoding map

For the encoding layer, we use the same procedure that we used for the previous algorithms [3], namely we map all input data  $x \in \mathbb{R}^n$  in  $[0, \frac{\pi}{2}]^n$ , and then we apply the encoding map

$$U_\phi : x \mapsto |\phi(x)\rangle = \bigotimes_{i=1}^n (\cos(x_i)|0\rangle + \sin(x_i)|1\rangle). \quad (1)$$

Note that several encoding maps are possible, some of them being more complex than the one we use. It is also possible to adapt data reuploading [19], in the sense that even if for a QCNN we progressively decrease the number of qubits, a solution would rather be to upload some of the features of the input data in every layer of the neural network. For this approach, one needs to identify what features to re-encode, so a feature importance analysis would be necessary.

### Convolutional and Pooling layers

The pooling layers reduce the number of qubits by entangling several qubits together and then tracing out some of them. We choose to use simple pooling gates, and to entangle the qubits pair-wise. The pooling gate that we use is described by the scheme in Figure 3a. The convolutional layers entangle qubits and use parameterized gates, that will be optimized during the algorithm. It may seem similar to the pooling layers, but the main difference is that the convolutional layer does not change the number of qubits used in the system. There are multiple possibilities in the choice of gates that one can use for this layer. Here we also choose a simple series of gates, as shown in Figure 3b.



Figure 3: Description of the convolutional and pooling layers used in our algorithm. In the pooling layer, the symbol  $\bullet$  means that the gate  $R_Z(\theta_1)$  is activated only if the first qubit is in the state  $|1\rangle$ . Conversely, the symbol  $\circ$  means that the gate  $R_X(\theta_2)$  is activated only if the first qubit is in the state  $|0\rangle$ . At the end of the pooling subcircuit we trace out the control qubit in order to reduce the dimension.

Note that even with the three gates of Figure 3b, we can implement a deeper convolutional layer by applying this two-qubits gate several times in the same layer, as in Figure 4. This also allows to entangle more qubits together.

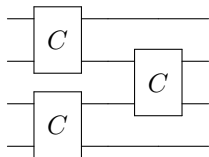


Figure 4: Example of another structure of convolutional layer

## Measure

At the end of the quantum circuit, we measure the last qubit in the Z-basis in order to obtain the expectation value  $\langle \Psi | \sigma_Z | \Psi \rangle$ . In other words, if we denote by  $U_\theta$  the matrix describing the quantum circuit, and if we define the observable  $\mathcal{O} = Z$ , we obtain

$$\langle \phi(x) | U_\theta^\dagger \mathcal{O} U_\theta | \phi(x) \rangle.$$

Having this expectation value is equivalent to having the probabilities of the quantum state to be in the state  $|0\rangle$  or in the state  $|1\rangle$ . Thus we can use it to compute a cost function, that will be minimized using a gradient-based method. In our case, we use the cross-entropy

$$C(\theta) = - \sum_{i=1}^N [y_i \log(\mathbb{P}(\Psi_i(\theta) = 1)) + (1 - y_i) \log(\mathbb{P}(\Psi_i(\theta) = 0))], \quad (2)$$

where  $y_i$  is the label associated to the  $i$ -th input data  $x_i$ , and where we measure the probabilities of the state  $|\Psi_i(\theta)\rangle = U_\theta |\phi(x_i)\rangle$  to be measured as 0 or 1. For the gradient-based method, we dispose of several methods, for instance the parameter shift rule [25] and the method called Simultaneous Perturbation for Stochastic Backpropagation (SPSB) [9], that we already used for the two previous tested quantum algorithms. In this article, we only use SPSB, as it is faster than the parameter shift rule and according to our observations [3] provides comparable results.

## Mathematical framework

We place ourselves in the framework of [20], to be sure that our algorithm will not suffer from Barren Plateaus. Thus, the gates in the convolutional layers can be defined as gates  $W_{i,j}^\ell(\theta^\ell)$  with

$$W_{i,j}^\ell(\theta^\ell) = e^{-i\theta_1^\ell H_1} e^{-i\theta_2^\ell H_2} V_{i,j},$$

where  $\ell$  represents the layer of the circuit,  $\theta^\ell = (\theta_1^\ell, \theta_2^\ell)$ ,  $H_k$  is a Hermitian operator such that  $e^{-i\theta_k^\ell H_k}$  is a parametrized single-qubit gate, and  $V_{i,j}$  is an unparametrized two-qubit gate (in our case a CNOT gate).

Concerning the pooling layer, the gates in the layers can be thought as maps from a two-qubit Hilbert space to a single-qubit Hilbert space. For a two-qubit state  $|\psi\rangle$ , the action of the pooling subcircuit is given by  $\psi_2 = \text{Tr}_1(P_{i,j}^\ell \psi)$ , with

$\text{Tr}_1$  being the partial trace over the Hilbert subspace corresponding to the first qubit, and where

$$P_{i,j}^\ell = |0\rangle\langle 0|_i U_{0,j}^\ell + |1\rangle\langle 1|_i U_{0,j}^\ell,$$

where  $U_{k,j}^\ell$  are parametrized single-qubit gates acting on the second register of  $|\psi\rangle$ . Finally, we measure the Z operator, corresponding to the Pauli-Z gate. We are in a very similar case to the one used in the numerical simulations of [20], thus the Corollary 1 of [20] can be applied and our quantum circuit will not exhibit Barren plateaus.

### 3 Reuploading circuit

#### 3.1 Motivations and description of the circuit

In this section we present a new architecture for the QCNN. Our thinking is that when the number of parameterized gates is too high compared to the number of features, the information given by the encoded data gets lost, thus the performances decrease. We want to use more information, without increasing the number of qubits. Hence, we adapt the concept of data reuploading [19], and reupload more information between each layer of the QCNN. As the number of qubits decreases between two layers, we do not make a choice in the data that we reupload but rather upload new information. For instance, when using a QCNN on 8 qubits (3 layers), we use a PCA 14 on the dataset, then encode the first 8 features before the first layer, the next 4 features between the first and second layers, and the last two features before the third layer. This procedure allows to increase the dimension of the PCA, and thus loose less information about the data: for a  $n$ -qubits circuit, we are able to use  $2(n - 1)$  features, whereas the standard procedure only used  $n$  features.

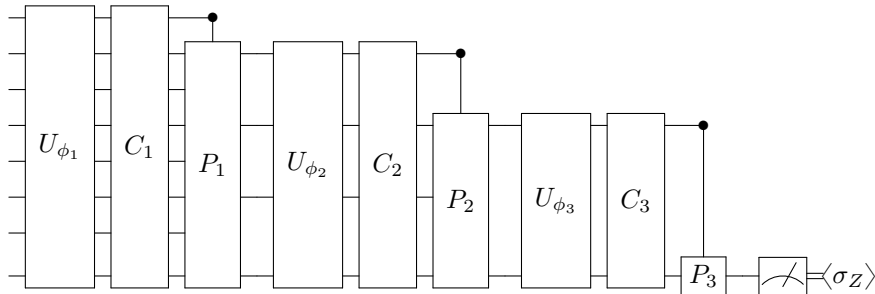


Figure 5: Description of our architecture for the layered uploading QCNN. We add an encoding layer before each convolutional layer, almost doubling the number of features injected in the quantum circuit.

### 3.2 Experiments and results

The main question about this new architecture is to know if it is indeed more efficient than the standard architecture with just one encoding layer at the beginning of the quantum circuit. Thus, our first experiment is to compare the two architectures on the well-known dataset MNIST, in order to classify images representing 0 and 1. We use five epochs for the training of our algorithms, on 10 000 data, gathering the accuracy score for each epoch, and then we gather the accuracy and F1 scores for the tests on 4 000 data. We compare the two architectures for different numbers of layers, namely from two to four layers.

| layers   | uploading | e1     | e2     | e3     | e4     | e5     | test(acc/F1)   |
|----------|-----------|--------|--------|--------|--------|--------|----------------|
| 2 layers | with      | 0.9695 | 0.98   | 0.9819 | 0.9774 | 0.9808 | 0.9837/0.9848  |
|          | without   | 0.9549 | 0.9795 | 0.9786 | 0.9787 | 0.9783 | 0.9742/0.9762  |
| 3 layers | with      | 0.9292 | 0.9701 | 0.9645 | 0.97   | 0.9652 | 0.983/0.9841   |
|          | without   | 0.8908 | 0.968  | 0.9661 | 0.9757 | 0.9685 | 0.97275/0.9746 |
| 4 layers | with      | 0.7102 | 0.9558 | 0.96   | 0.9607 | 0.9577 | 0.9795/0.9809  |
|          | without   | 0.7821 | 0.96   | 0.9709 | 0.9737 | 0.9706 | 0.97725/0.9789 |

Table 2: Comparison of the two architectures for different layers on the MNIST dataset, classifying images of 0 and 1.

As we can see, the new architecture performs better in every model, in terms of accuracy or F1 scores. If we look at the training performances, sometimes the model without uploading gets better results, but since in the test it is not the case it could suggest some overfitting phenomenon. Note also that the model performances seems to decrease with the number of layers, which tends to confirm our intuition that the information from the input data may get lost when there are too many parameters in the quantum circuit.

These results show that our architecture increases the performances of the QCNN model. However, the difference between the scores of two architectures is quite thin, and we would like to see if for more complex cases it becomes more significant. Thus we try a second test on the MNIST dataset. This time we want to classify images corresponding to 0 and 8, which are graphically closer numbers than 0 and 1.

| layers   | uploading | e1     | e2     | e3     | e4     | e5     | test(acc/F1)  |
|----------|-----------|--------|--------|--------|--------|--------|---------------|
| 2 layers | with      | 0.945  | 0.938  | 0.953  | 0.965  | 0.963  | 0.9547/0.9548 |
|          | without   | 0.946  | 0.960  | 0.934  | 0.961  | 0.965  | 0.9512/0.9518 |
| 3 layers | with      | 0.8992 | 0.9548 | 0.9578 | 0.947  | 0.9499 | 0.958/0.9579  |
|          | without   | 0.9138 | 0.9544 | 0.9499 | 0.9469 | 0.9328 | 0.9495/0.9500 |
| 4 layers | with      | 0.5265 | 0.5198 | 0.7798 | 0.9454 | 0.9454 | 0.926/0.928   |
|          | without   | 0.8264 | 0.9517 | 0.9447 | 0.9596 | 0.9530 | 0.944/0.9449  |

Table 3: Comparison of the two architectures for different layers on the MNIST dataset, classifying images of 0 and 8.

On this table we can see the same phenomenon, namely that the model

with the layered uploading performs better than the model without layered uploading. The differences between the scores of the two models do not seem to be greater than for the previous test, the gain being around 1% for both tasks, which is not negligible for this kind of datasets. For this second classification task, we note that the scores are smaller than when we classify 0 and 1; it can be explained quite simply by the fact that 0 and 8 are graphically closer than 0 and 1, especially with a low dimension of PCA which tends to blur the images. We can see that for the biggest model, namely for four layers, our model does not perform better than the standard model which could be due to several things. First the model seems to struggle to learn in the first epochs, so maybe five epochs is not enough to reach a good model. Second, maybe the additional features in the model with uploading tend to fool the algorithm, which makes the learning phase more difficult. In order to verify these hypotheses, we first run the two models on 10 epochs. On Table 4, we can see that when we let to the algorithm the "time" to learn properly, it indeed performs better than the basic QCNN, with in our case a difference of 4% in both accuracy and F1-score. As an additional test, we run a standard five-layers model, which takes into account a comparable number of features as the four-layers model with layered uploading, but with a lot more free parameters. The results, presented in Table 5, are very bad for this model, so it confirms that our architecture could be preferable in order to take more features into account.

|         |         |         |         |         |          |               |
|---------|---------|---------|---------|---------|----------|---------------|
|         | epoch 1 | epoch 2 | epoch 3 | epoch 4 | epoch 5  |               |
| with    | 0.6596  | 0.9450  | 0.9427  | 0.9385  | 0.9385   |               |
| without | 0.7693  | 0.9218  | 0.9407  | 0.9390  | 0.9480   |               |
|         | epoch 6 | epoch 7 | epoch 8 | epoch 9 | epoch 10 | test (acc/F1) |
| with    | 0.9356  | 0.9259  | 0.9356  | 0.9405  | 0.9347   | 0.9625/0.9605 |
| without | 0.9466  | 0.9387  | 0.9439  | 0.9276  | 0.9478   | 0.924/0.9267  |

Table 4: Comparison of the two architectures for 4 layers and 10 epochs on the MNIST dataset, classifying images of 0 and 8.

|          |         |         |         |         |         |               |
|----------|---------|---------|---------|---------|---------|---------------|
|          | epoch 1 | epoch 2 | epoch 3 | epoch 4 | epoch 5 | test(acc/F1)  |
| 5 layers | 0.5055  | 0.5087  | 0.4984  | 0.5152  | 0.4935  | 0.4817/0.6138 |

Table 5: 5 layers model without layered uploading, classifying images of 0 and 8 on the MNIST dataset.

Finally, we want to test the efficiency of our architecture on the dataset which is important to us, namely the malware images dataset. Since this dataset is made of images of files, which are very noisy (see Figure 1), the classification task seems even harder than previously. The dimension of the PCA thus should play a very important role, and we want it as high as possible without increasing the number of qubits too much. To deal with this dataset, we compute the F1-score for both training and test, because it is a more robust metric when it

comes to unbalanced datasets. We also compute the accuracy scores, which are postponed in the Appendix.

| layers   | uploading | e1     | e2     | e3     | e4     | e5     | test   |
|----------|-----------|--------|--------|--------|--------|--------|--------|
| 2 layers | with      | 0.6464 | 0.6798 | 0.6940 | 0.7174 | 0.7036 | 0.780  |
|          | without   | 0.6409 | 0.7063 | 0.7042 | 0.6998 | 0.6996 | 0.7698 |
| 3 layers | with      | 0.6195 | 0.6784 | 0.6835 | 0.6528 | 0.6547 | 0.785  |
|          | without   | 0.4525 | 0.4665 | 0.5933 | 0.5294 | 0.5049 | 0.5897 |

Table 6: F1-score comparison of the two architectures for different layers on the malware dataset, classifying images of malware and benign files.

|         | epoch 1 | epoch 2 | epoch 3 | epoch 4 | epoch 5 |
|---------|---------|---------|---------|---------|---------|
| with    | 0.4578  | 0.4165  | 0.5555  | 0.4596  | 0.5708  |
| without | 0.5105  | 0.4877  | 0.5304  | 0.5406  | 0.3813  |

|         | epoch 6 | epoch 7 | epoch 8 | epoch 9 | epoch 10 | test   |
|---------|---------|---------|---------|---------|----------|--------|
| with    | 0.4961  | 0.5141  | 0.5119  | 0.5427  | 0.5427   | 0.6625 |
| without | 0.4580  | 0.5901  | 0.5931  | 0.4243  | 0.5936   | 0.6737 |

Table 7: F1-score comparison of the two architectures for 4 layers and 10 epochs on the malware dataset, classifying images of malware and benign files.

For the models with two and three layers in Table 6, we observe once again that circuit with layered uploading performs better on the F1-score: 1% for two layers, and a lot more for the three-layers model. For this last one, we even can see that the training without layered uploading is not efficient at all, and thus the model performs poorly on the test. This might be due to the number of parameters which is too big compared to the number of features injected in the circuit, which themselves are maybe not meaningful enough. This model is a very good example of the utility of our architecture, which allows to have a good learning phase even with three layers and low-impact features. For the bigger model, we increase the training phase to 10 epochs, and we gather the results on Table 7. For this model, our architecture does not provide any improvement, neither in accuracy nor F1-score. However, both of the algorithms perform poorly in the detection task, reaching less than 68% in F1-score. Thus we can consider that the added features are not impacting enough to make a difference, and that the number of free parameters is too big compared to the number of features, so that the information about the files might get lost in the quantum circuit. Besides, the PCA may not be a suitable solution for the feature reduction, because it does not give us any information on the relevance of these new features. Moreover, in our use-case, we classify images of PE files, composed of different specific sections, with specific features, which are mixed up all together when applying the PCA. A deeper analysis of the structure of our dataset with standard QCNNS can be found in [21].

When the size of the quantum circuit increases, initialization of parameters becomes important. Even if in our case we do not exhibit Barren plateaus,

a bad initialization could slow down the learning phase, and thus give poor results. We try to initialize all our parameters to 0, and then to  $2\pi$ , in order to start the training with the identity operator, but it did not increase the model’s performances. Finally, the size of the dataset is certainly a problem: one should consider a lot more than 10,000 files to train the algorithms. However, our aim being to be able to extract useful information for little datasets, with few features, we did not explore this lead, because of the computation time problematic, and especially because our architecture gave good results for all the tested models but this last one.

## Conclusion

In a nutshell, we proposed in this paper a new architecture for quantum convolutional neural networks, allowing to encode more features without increasing the size of the quantum circuit. It is inspired from data reuploading and consists in adding an encoding layer composed of new features before each convolutional layer. With this approach, one can use  $2(n - 1)$  features for a  $n$ -qubits circuit, so it almost doubles the information that is given to the QCNN. We compared our architecture with a standard QCNN on several classification tasks, namely classifying 0 and 1 then 0 and 8 from the MNIST dataset, and classifying malware and benign files from our personal dataset. On all our tests except one this new architecture presented better performances than the standard one, so we believe it is a relevant method to use the information that we can gather from data without systematically increase the size of our dataset or the size of the algorithm. This work might for instance allow us to enhance our models using QCNNs as presented in [21] in order to get a better detection rate and a greater knowledge about malware PE files.

There are several leads that could be investigated in order to continue our work on this architecture. First we did not focus on the convolutional and pooling layers: maybe some other choices of gates would allow better performances for our use-cases. Computing the Lie algebra generated by each layer could give us information about the expressiveness of our model, as it has been shown to be an important tool for QNNs [12, 17, 24]. Concerning the encoding of the features itself, we think that our limits mainly came from the fact that the PCA method does not give information about the output features, so it is hard to know if we encode the features in the right way in the quantum circuit. One solution would be to identify in a first time the most important features, and then reorganize the way that we encode them in the circuit. Besides, if some features are largely more impacting than others, one could try to re-encode them all along the algorithm (for example in each encoding layer). Finally, even if it is not in our concern yet because of the current capacities of quantum computers, it would be good to pursue our tests on bigger models an bigger datasets to see if it makes a real difference in the learning of QCNNs.

## References

- [1] Amira Abbas, David Sutter, Christa Zoufal, Aurelien Lucchi, Alessio Figalli, and Stefan Woerner. The power of quantum neural networks. *Nature Computational Science*, 1(6):403–409, jun 2021.
- [2] Hyrum Anderson and Phil Roth. Ember: An open dataset for training static pe malware machine learning models. 04 2018.
- [3] Grégoire Barrué and Tony Quertier. Quantum machine learning for malware classification. *arXiv preprint arXiv:2305.09674*, 2023.
- [4] Denis Bokhan, Alena S. Mastiukova, Aleksey S. Boev, Dmitrii N. Trubnikov, and Aleksey K. Fedorov. Multiclass classification using quantum convolutional neural networks with hybrid quantum-classical learning. *Frontiers in Physics*, 10, nov 2022.
- [5] M. Cerezo, Guillaume Verdon, Hsin-Yuan Huang, Lukasz Cincio, and Patrick J. Coles. Challenges and opportunities in quantum machine learning. *Nature Computational Science*, 2(9):567–576, sep 2022.
- [6] Iris Cong, Soonwon Choi, and Mikhail D Lukin. Quantum convolutional neural networks. *Nature Physics*, 15(12):1273–1278, 2019.
- [7] Daniel Gibert, Carles Mateu, and Jordi Planes. The rise of machine learning for detection and classification of malware: Research developments, trends and challenges. *Journal of Network and Computer Applications*, 153(January):102526, 2020.
- [8] Edward Grant, Leonard Wossnig, Mateusz Ostaszewski, and Marcello Benedetti. An initialization strategy for addressing barren plateaus in parametrized quantum circuits. *Quantum*, 3:214, December 2019.
- [9] Thomas Hoffmann and Douglas Brown. Gradient estimation with constant scaling for hybrid quantum machine learning, 2022.
- [10] Zoë Holmes, Kunal Sharma, M. Cerezo, and Patrick J. Coles. Connecting ansatz expressibility to gradient magnitudes and barren plateaus. *PRX Quantum*, 3(1), jan 2022.
- [11] Tak Hur, Leeseok Kim, and Daniel K. Park. Quantum convolutional neural network for classical data classification. *Quantum Machine Intelligence*, 4(1), feb 2022.
- [12] Martin Larocca, Nathan Ju, Diego García-Martín, Patrick J. Coles, and M. Cerezo. Theory of overparametrization in quantum neural networks, 2021.
- [13] Michael Lester. Practical Security Analytics - PE Malware Machine Learning Dataset. <https://practicalsecurityanalytics.com/pe-malware-machine-learning-dataset/>.

- [14] Benjamin Marais. *Améliorations des outils de détection de malwares par analyse statique grâce à des mécanismes d'intelligence artificielle*. PhD thesis, Normandie, 2023.
- [15] Benjamin Marais, Tony Quertier, and Stéphane Morucci. Ai-based malware and ransomware detection models. In *Conference on Artificial Intelligence for Defense*, 2022.
- [16] Jarrod R. McClean, Sergio Boixo, Vadim N. Smelyanskiy, Ryan Babbush, and Hartmut Neven. Barren plateaus in quantum neural network training landscapes. *Nature Communications*, 9(1), nov 2018.
- [17] Johannes Jakob Meyer, Marian Mularski, Elies Gil-Fuster, Antonio Anna Mele, Francesco Arzani, Alissa Wilms, and Jens Eisert. Exploiting symmetry in variational quantum machine learning, 2022.
- [18] L Nataraj, S Karthikeyan, G Jacob, and B S Manjunath. Malware images: Visualization and automatic classification. In *ACM International Conference Proceeding Series*, 2011.
- [19] Adrián Pérez-Salinas, Alba Cervera-Lierta, Elies Gil-Fuster, and José I. Latorre. Data re-uploading for a universal quantum classifier. *Quantum*, 4:226, feb 2020.
- [20] Arthur Pesah, M. Cerezo, Samson Wang, Tyler Volkoff, Andrew T. Sornborger, and Patrick J. Coles. Absence of barren plateaus in quantum convolutional neural networks. *Physical Review X*, 11(4), oct 2021.
- [21] Tony Quertier and Grégoire Barraué. Towards an in-depth detection of malware using distributed qcnn, 2023.
- [22] Edward Raff, Jon Barker, Jared Sylvester, Robert Brandon, Bryan Catanzaro, and Charles K Nicholas. Malware detection by eating a whole exe. In *Workshops at the thirty-second AAAI conference on artificial intelligence*, 2018.
- [23] Edward Raff and Charles Nicholas. A Survey of Machine Learning Methods and Challenges for Windows Malware Classification. 2020.
- [24] Michael Ragone, Bojko N. Bakalov, Frédéric Sauvage, Alexander F. Kemper, Carlos Ortiz Marrero, Martin Larocca, and M. Cerezo. A unified theory of barren plateaus for deep parametrized quantum circuits, 2023.
- [25] Maria Schuld, Ville Bergholm, Christian Gogolin, Josh Izaac, and Nathan Killoran. Evaluating analytic gradients on quantum hardware. *Physical Review A*, 99(3), mar 2019.
- [26] Sukin Sim, Peter D. Johnson, and Alán Aspuru-Guzik. Expressibility and entangling capability of parameterized quantum circuits for hybrid quantum-classical algorithms. *Advanced Quantum Technologies*, 2(12):1900070, oct 2019.

- [27] Daniele Ucci, Leonardo Aniello, and Roberto Baldoni. Survey of machine learning techniques for malware analysis. *Computers and Security*, 81:123–147, 2019.
- [28] Chukwudubem Umeano, Annie E. Paine, Vincent E. Elfving, and Oleksandr Kyriienko. What can we learn from quantum convolutional neural networks?, 2023.
- [29] Roeland Wiersema, Cunlu Zhou, Yvette de Sereville, Juan Felipe Carrasquilla, Yong Baek Kim, and Henry Yuen. Exploring entanglement and optimization within the hamiltonian variational ansatz. *PRX Quantum*, 1(2), December 2020.
- [30] Limin Yang, Arridhana Ciptadi, Ihar Laziuk, Ali Ahmadzadeh, and Gang Wang. BODMAS: An Open Dataset for Learning based Temporal Analysis of PE Malware. In *Proceedings - 2021 IEEE Symposium on Security and Privacy Workshops, SPW 2021*, pages 78–84, 2021.

## 4 Appendix

This appendix gathers some the tests that we have done for our architecture on the malware dataset. In the previous sections we only presented results about F1-score for this dataset because it makes more sense, but here are the same tests with the accuracy scores. Table 8 gives us the results for the models with two and three layers, while Table 9 shows the results of the ten epoch on the four layer model.

| layers   | uploading | e1     | e2     | e3     | e4     | e5     | test   |
|----------|-----------|--------|--------|--------|--------|--------|--------|
| 2 layers | with      | 0.6244 | 0.6982 | 0.6774 | 0.7065 | 0.7018 | 0.7447 |
|          | without   | 0.6485 | 0.693  | 0.6955 | 0.6955 | 0.6948 | 0.7592 |
| 3 layers | with      | 0.539  | 0.6529 | 0.6549 | 0.5953 | 0.6335 | 0.744  |
|          | without   | 0.5011 | 0.5211 | 0.5313 | 0.516  | 0.5434 | 0.5157 |

Table 8: Accuracy comparison of the two architectures for different layers on the malware dataset, classifying images of malware and benign files.

|         | epoch 1 | epoch 2 | epoch 3 | epoch 4 | epoch 5 |
|---------|---------|---------|---------|---------|---------|
| with    | 0.4957  | 0.4978  | 0.5026  | 0.5057  | 0.5119  |
| without | 0.5068  | 0.4847  | 0.4949  | 0.4978  | 0.5013  |

|         | epoch 6 | epoch 7 | epoch 8 | epoch 9 | epoch 10 | test   |
|---------|---------|---------|---------|---------|----------|--------|
| with    | 0.4968  | 0.5039  | 0.4925  | 0.5085  | 0.5021   | 0.5025 |
| without | 0.4976  | 0.5118  | 0.4985  | 0.5063  | 0.5713   | 0.5547 |

Table 9: Accuracy comparison of the two architectures for 4 layers and 10 epochs on the malware dataset, classifying images of malware and benign files.